Soft Matter

PAPER

View Article Online
View Journal | View Issue

Cite this: *Soft Matter*, 2022, **18**, 6404

Programming interactions in magnetic handshake materials†

Chrisy Xiyu Du, *[a] Hanyu Alice Zhang,[b] Tanner G. Pearson,[c] Jakin Ng,[c] Paul L. McEuen,[cd] Itai Cohen[cd] and Michael P. Brenner[a]

The ability to rapidly manufacture building blocks with specific binding interactions is a key aspect of programmable assembly. Recent developments in DNA nanotechnology and colloidal particle synthesis have significantly advanced our ability to create particle sets with programmable interactions, based on DNA or shape complementarity. The increasing miniaturization underlying magnetic storage offers a new path for engineering programmable components for self assembly, by printing magnetic dipole patterns on substrates using nanotechnology. How to efficiently design dipole patterns for programmable assembly remains an open question as the design space is combinatorially large. Here, we present design rules for programming these magnetic interactions. By optimizing the structure of the dipole pattern, we demonstrate that the number of independent building blocks scales super linearly with the number of printed domains. We test these design rules using computational simulations of self assembled blocks, and experimental realizations of the blocks at the mm scale, demonstrating that the designed blocks give high yield assembly. In addition, our design rules indicate that with current printing technology, micron sized magnetic panels could easily achieve hundreds of different building blocks.

Received 9th May 2022,
Accepted 8th August 2022

DOI: 10.1039/d2sm00604a

rsc.li/soft-matter-journal

1 Introduction

A key feature of living materials is the inherent programmability of their parts. Complex assemblies require that components with low crosstalk bind to desired partners without binding to others.[1] Such programmability is at the core of biochemical functionality, from protein folding[2,3] to self assembly of catalytic protein complexes[4,5] or multicomponent molecular machines.[6,7] Biology has managed to create a robust interaction set from a limited set of nucleic and amino acids. Major advances have been made in the engineering of specific interactions that use these biological solutions, by either directly programming nucleic acid assembly[8,9] or by using them as specific glues coating nanoparticles[10,11] or colloids.[12,13] However, these interactions can be hard to program as they are all based on hydrogen bonds, which have a fixed binding energy strength. An alternative solution for designing programmable building blocks are magnetic handshake materials[14] whose interactions are governed by magnetic dipole patterns (Fig. 1). Importantly, there is extensive prior literature on the phase behaviors of magnetic spheres,[22–25] network structure formation by external driving forces[26–29] and the influence of particle shape on assembly.[30] These studies, however, focused on building blocks with a single magnetic dipole. In the magnetic handshake materials studied here, multiple dipoles encode the information for binding. Such materials can be made over a range of size scales, extending to the nanoscale, where, bootstrapping off Moore's law-like advances in magnetic recording technologies,[15–18] nanotechnology can be used to print magnetic dipoles on substrates. This

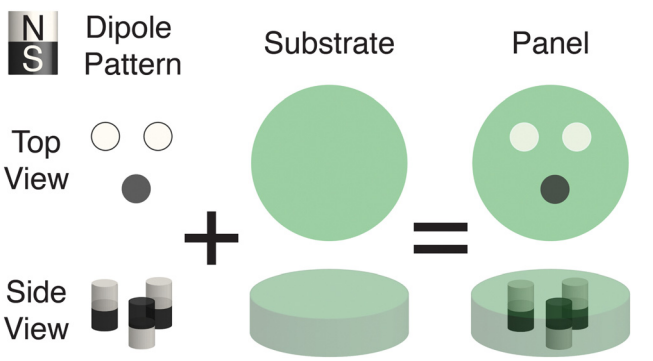

Fig. 1 Illustration of general design principle of magnetic handshake panels. We encode information of specific binding by printing dipole patterns, specifying location and orientation of magnetic dipoles, on substrates.

[a] *School of Engineering and Applied Sciences, Harvard University, Cambridge, MA, 02139, USA. E-mail: xiyudu@seas.harvard.edu*
[b] *School of Applied and Engineering Physics, Cornell University, Ithaca, NY, 14853, USA*
[c] *Department of Physics, Cornell University, Ithaca, NY, 14853, USA*
[d] *Laboratory of Atomic and Solid-State Physics, Cornell University, Ithaca, NY, 14853, USA*

† Electronic supplementary information (ESI) available. See DOI: https://doi.org/10.1039/d2sm00604a

technology offers an information rich substrate for programming interactions between building blocks to create novel materials, with a potentially large number of programmable building blocks. Dipole patterns can vary in both their strength and their spatial distribution. Over the past decade, bit sizes have approached 30 nm, the fundamental stability limit of magnetic domains,[19–21] giving us a combinatorially large space to design interactions.

The major goal of this paper is to elucidate the basic rules for programming building blocks from magnetic printing. For a given building block design, we need to determine the positions and strengths of the magnetic domains to maximize programmability. We find these programming rules by combining information theory[31] with physical modeling. Magnetic interactions are simple to describe mathematically and are easy to model, in contrast to electrostatic and chemical interactions. The absence of magnetic monopoles eliminates the complicated screening charge configurations that plague quantitative modeling of electrostatic systems. This simplification makes design iteration computationally efficient and highly predictive.

2 Model and method

Information capacity formalism of lock-key binding pairs

The central design requirement for programmability is finding building blocks with low crosstalk. For a system in thermodynamic equilibrium, the yield of an undesired configuration decays exponentially with its energy gap Δ from the desired configuration.[31] Designing for low crosstalk therefore requires calculating the distribution of binding energies for the components, and optimizing the Δ distribution to maximize the yield of the desired configuration.

To formulate this optimization problem in terms of the basic building blocks, we consider a set of lock and key pairs, denoted as $x_1, x_2, \ldots, x_M \in X$ for locks, and $y_1, y_2, \ldots, y_M \in Y$ for keys, with the binding energy matrix E, where $E_{ij} \equiv E(x_i, y_j)$. Assuming locks and keys have the same concentrations, the equilibrium probability of the lock i to bind the key j is $p(x_i, y_j) = e^{-\beta E_{ij}}/Z$, where β is the inverse thermal energy and Z is the partition function. A natural metric for quantifying cross talk is mutual information,[31] given by

$$I(X;Y) = \sum_{x_i \in X, y_j \in Y} p(x_i, y_j) \log \frac{p(x_i, y_j)}{p(x_i)p(y_j)}. \quad (1)$$

Maximizing the mutual information $I(X; Y)$ over the sets of locks and keys X, Y minimizes the cross talk. The set with the optimal information capacity $I_c = \max(I)$ has effectively $M_c = \exp(I_c)$ non-crosstalking lock-key pairs.

Using the general theoretical framework developed in ref. 31, we lay out the information capacity computation here for the magnetic handshake system. For a system with a well-defined number of lock and key building blocks and binding energy matrix E, we can directly calculate M_c from eqn (1). For experimental systems without a set number of locks and keys, we can calculate M_c by first computing the energy gap distribution Δ based on binding energy matrices of random sampled components (see details in (ESI†)). We define Δ as $\Delta_{ij} = E_{ij} - s_{ii}$, where s_{ii} is the strength of the on-target binding of lock i and key i and E_{ij} is the off-target binding energy between lock i and key j. Denoting $\rho(\Delta)$ as the distribution of gap energies between on target and off target binding, the maximal number of non-crosstalking pairs (M_c) is given by[31]

$$M_c = \frac{(1 + \langle e^{-\beta\Delta}\rangle)^2}{\langle \beta\Delta e^{-\beta\Delta}\rangle - \langle e^{-\beta\Delta}\rangle + \langle e^{-\beta\Delta}\rangle^2}, \quad (2)$$

where $\langle\cdot\rangle$ is the average with respect to $\rho(\Delta)$. This formula is intuitive: if we consider the (exponentially weighted) average of the gap Δ much larger than k_BT so that $\beta\Delta \gg 1$, then M_c increases *exponentially* with Δ as

$$M_c \sim (\langle \beta\Delta e^{-\beta\Delta}\rangle)^{-1}. \quad (3)$$

Using this framework, we can directly formulate an optimization problem of how to encode dipole patterns for a set of magnetic building blocks to maximize programmability. Here, we measure programmability by evaluating M_c of a set of magnetic patterns, the larger the M_c, the better the programmability. Given a potential design for a set of magnetic dipoles on a substrate, we can compute the distribution of gap energies $\rho(\Delta)$, and thus the effective number M_c of programmable building blocks (eqn (2)).

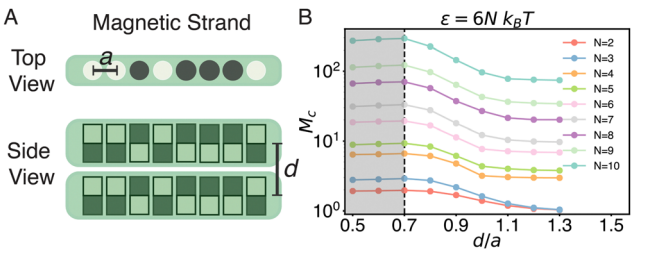

Fig. 2 1D Magnetic strand with fixed single dipole–dipole binding energy. (A) Sample configuration of a magnetic strand with $N = 8$ dipoles. The distance between any two nearest neighbor dipoles on the same strand is denoted as a, while the interaction distance between two different strands is denoted as d. (B) The largest effective number (M_c) of strands with no crosstalk for magnetic strands of length $N = 2$–10 with different d/a ratio. Beyond $d/a = 0.7$, we find that M_c rapidly decreases. Here, we use $\varepsilon = 6Nk_BT$ to show the maximum effect on M_c varying d/a ratio.

Magnetic interaction model

Magnetic interactions between any two panels depend on the spatial configuration of their dipoles, and in particular the ratio d/a, where a is the center to center distance between adjacent dipoles on the same panel, and d is the distance between the centerlines of two panels (Fig. 2A). By summing over the interactions between every dipole pair on different panels, we can write down the binding energy for on-target binding between two complementary magnetic panels (see (ESI†) for detailed derivation).

$$V = -\frac{\mu_0 m^2}{2\pi d^3}\left[N + k \cdot \frac{d^3}{a^3} \cdot \frac{2d^2/a^2 - 1}{(1 + d^2/a^2)^{5/2}} + \mathscr{F}\left(\frac{d}{a}\right)\right] \quad (4)$$

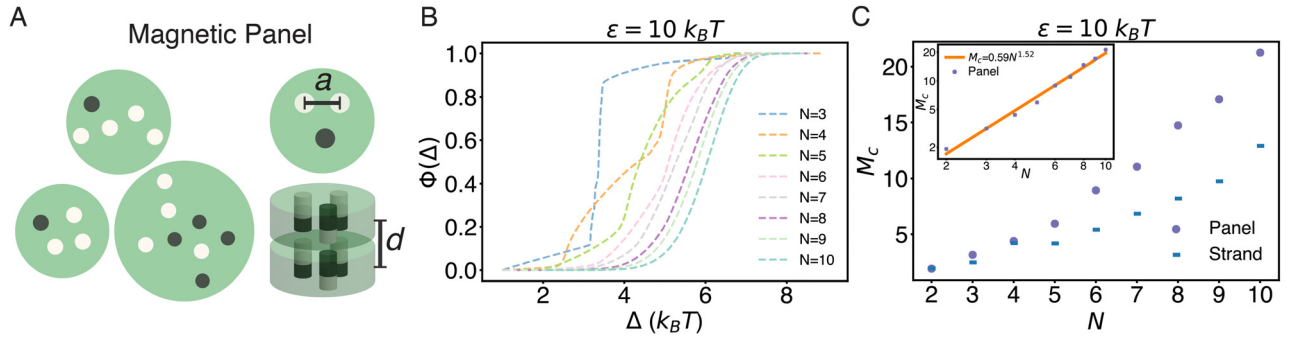

Fig. 3 2D magnetic panel with fixed total binding energy. (A) Three sample dipole patterns with number of dipoles N = 4, 5, 8. The dipoles are placed with the constraint that all nearest neighbor distances for any two dipole pairs must be the same. (B) The cumulative distribution functions of Δ for magnetic panels with N = 3–10 dipoles with total binding energy $\varepsilon = 10k_BT$. (C) M_c of magnetic panels and strands with N dipoles for $\varepsilon = 10k_BT$. We see that by allowing the placement of dipoles on a 2D plane, we increased information capacity of our system. The insert shows the scaling behavior of M_c as a function of N dipoles for panels at $\varepsilon = 10k_BT$. We note that at $\varepsilon = 10k_BT$, M_c increases super linearly as a function of N.

Here μ is vacuum permeability, m is the magnitude of the magnetic dipole moments, N is the number of dipoles on a single panel, k is the number of second-nearest neighbor aligned dipole pairs minus the anti-aligned dipole pairs, and $\mathscr{F}$ is the (negligible) effect of third or higher neighbor interactions. eqn (4) implies that the second-nearest neighbor term vanishes when $2d^2/a^2 = 1$, corresponding to the case where a dipole's magnetic field is perpendicular to its next nearest neighbor. Even though dipole–dipole interaction is long range,[32] at $d/a = \sqrt{2}/2$, the majority of the binding energy contributions between two magnetic panels come from nearest neighbor interactions, while the higher order terms mark around 2% of the binding energies (see (ESI†) for more detail).

1D magnetic strands

To test whether the separation ratio of $d/a = \sqrt{2}/2$ gives rise to a higher information capacity of magnetic panels, we first consider a one dimensional chain of magnetic dipoles, where we can systematically enumerate the entire configuration space of 2^N dipole strands with N dipoles. When generating the distinct dipole strand, we remove palindromic sequences corresponding to the same lock-key pair, such as NNNNSSSS and SSSSNNNN. We enumerate the number of non-palindromic strands for $L \in [2, 10]$ giving [2, 3, 7, 10, 21, 36, 78, 136, 327] distinct patterns. Using eqn (1), we directly compute M_c as a function of d/a, by calculating the binding energy matrices of all possible magnetic strands (Fig. 2B). We find that the information capacity M_c decreases rapidly beyond $d/a \sim 0.7$, confirming our hypothesis that the magnetic strand system has higher information capacity by eliminating second-nearest neighbor interactions.

Fig. 2B shows that M_c increases exponentially with the number N of dipoles, arising due to the exponential dependence of M_c on the energy gap Δ (eqn (3)). Since we computed M_c values by fixing the strength of the individual dipoles, both the on target binding energy and the distribution of energy gap increases linearly with N, resulting an exponential increase of M_c. This energy dependence highlights a fundamental constraint for programmability. The timescale of unbinding increases exponentially with interaction strength. Practical design requires the unbinding timescale to be much smaller than the experimental timescale, as otherwise the system will be trapped in non-desired configurations. Given the timescale of an experiment, we need to choose the binding strengths to be small enough for this condition to be satisfied. Therefore, the correct optimization problem is to maximize the number of components for a fixed total binding energy.

2D magnetic panels

We now turn to the design of dipole configurations on two dimensional panels. We fix the total on-target binding energy ε between any two building blocks to be $10k_BT$, so a panel with 3 dipoles has individual dipoles with a magnetic moment that is $\sqrt{10/3}$ the dipole moment in a 10-dipole panel. We consider placements of dipoles on the plane, keeping the constraint $d/a = \sqrt{2}/2$. We compute $\rho(\Delta)$ by random sampling, over configurations where every dipole has at least one nearest neighbor of distance a, with no nearest neighbors smaller than a (Fig. 3A). Using a randomly generated magnetic pattern library, we calculate the equilibrium configuration and total binding energy E_{ij} for each pair of panels in the library.

Fig. 3B shows the cumulative distribution function for 2D panels with N = 3–10 dipoles, where we fixed the total binding energy between building blocks to be $10k_BT$. The energy gap between on and off target binding increases with increasing N. Fig. 3C compares M_c of 1D strands and 2D panels at fixed total binding energy of $\varepsilon = 10k_BT$, where the 2D panels contain much more information. In addition, the insert of Fig. 3C shows that $M_c \sim N^{1.5}$ for $\varepsilon = 10k_BT$, namely the number of effective components increases super linearly with N. This scaling means that even with fixed binding energy between components, we can increase the programmability of our system by printing more magnetic dipoles. This is important, as it suggests that increase in magnetic storage information density can directly result in an increase in information content of panels for assembly without changing the timescale for unbinding.

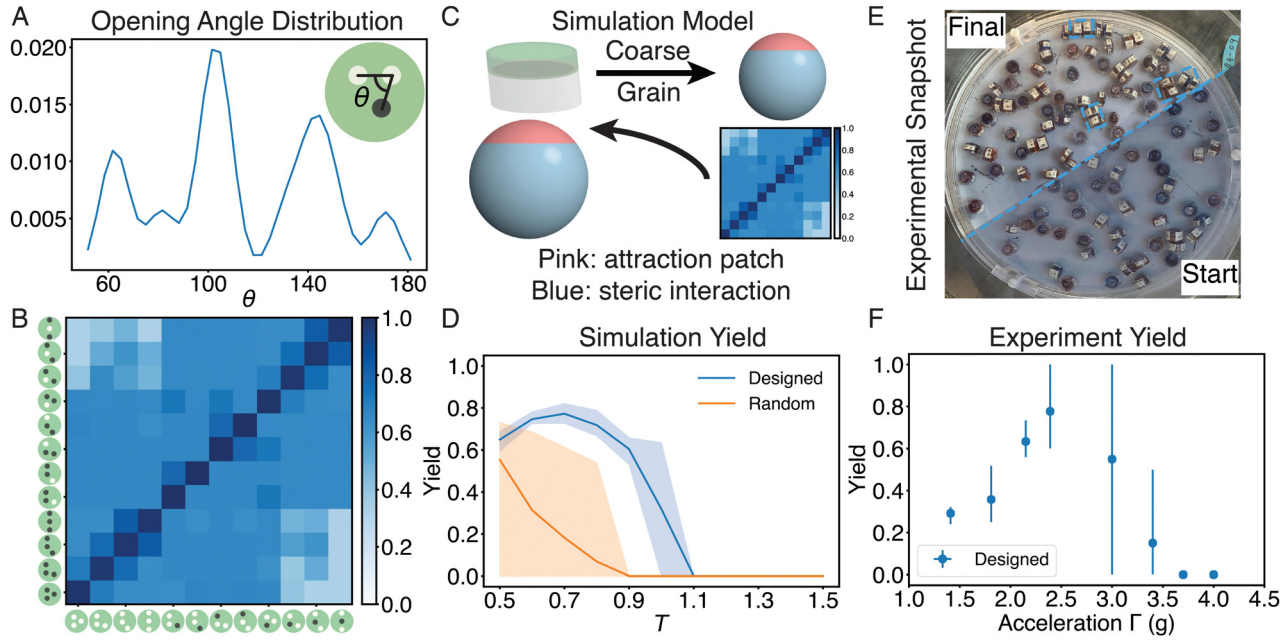

Fig. 4 Dimer assembly: (A) The opening angle (θ) distribution for the high information 3-dipole panels before optimization. (B) The binding energy matrix of the designed 3-dipole panels. The binding energies are scaled with the strongest binding energy of the 12 lock-key pairs. (C) The coarse grain process of converting a magnetic panel to a sphere with an attractive patch for simulation. (D) The self-assembly yield of the designed panels compare to the randomly generated ones (not obeying fixed d/a ratio) as a function of simulation temperature. (E) Start and final state from shaker experiment. Dimers in blue rectangles form the desired lock-key pairs. (F) The self-assembly yield of the designed panels as a function of shaker acceleration (unit in gravitational acceleration g).

Practically, the shortest side of a magnetic region must be bigger that ~30 nm to ensure permanence. This limit sets a natural cutoff for the minimum size and strength of a domain.

3 Self-assembly results

Dimer self-assembly

To validate that the designed dipole patterns can accurately assemble, we carry out both molecular dynamics simulations and experiments comparing the yield of dimer assembly between designed and randomly generated 3-dipole patterns. In the simulations the total on-target binding energy was set to $10k_BT$. For the experiments, we used panels with N40 Neodymium magnets separated by a = 0.28 cm and binding distance d = 0.2 cm, and varied the shaker acceleration to control the effective temperature of the system. We find the best patterns of 3 dipoles by iterating through randomly generated patterns, selecting those with high information content. We then applied symmetry analysis by measuring the opening angle θ (Fig. 4A) distribution on all the patterns and identified the optimal symmetries for the best patterns (θ peaks around 60, 100, 140, and 180 degrees). Lastly, we generated patterns with said symmetries and iterated over different dipole configurations to get the final designed patterns (Fig. 4B). The design protocol yields 12 distinct lock-key pairs (Fig. 4B) with M_c = 3.46 at $\varepsilon = 10k_BT$, implying that a theoretical binding yield of about 68%.

We instantiate these designed configurations in both simulations and experiments, printing the lock-key pairs onto dimers. We carry out the simulations in HOOMD-blue,[33–35] while we used Freud[36] for data analysis, and Signac[37,38] for data management (More detailed description of the simulation setup can be found in the (ESI†)). We program the interactions between lock-key dimers by putting a small interaction patch on a sphere with the computed binding energy (Fig. 4C). The patch is small enough to ensure that only dimers can form in our simulation (see (ESI†) for simulation snapshots). We carry out an ensemble of five different runs of the dimer simulations as a function of temperature, measuring the yield of the desired configurations. We compare this yield curve to that computed from 15 sets of randomly generated panels. Fig. 4D shows that the designed panels have significantly higher yield than the random panels, with a maximum yield nearly 80%.

For the experiments, we followed a similar protocol. We super glued magnets into laser cut holders and made them into cylindrical panels following the theoretical designs. We placed these 4 copies of each lock-key pair into a shaker, and measured dimer assembly as a function of shaking amplitude. The lock-key pairs are fabricated with specific dimensions so that the binding energy is only substantial when they bind face to face (see more detail in (ESI†)). The shaking is analogous to the temperature of a thermal bath, providing uncorrelated noise to the individual panels (more details for the shaker system setup can be found in ESI†). The number of pairs of each dipole pattern is determined to match the simulation area fraction of

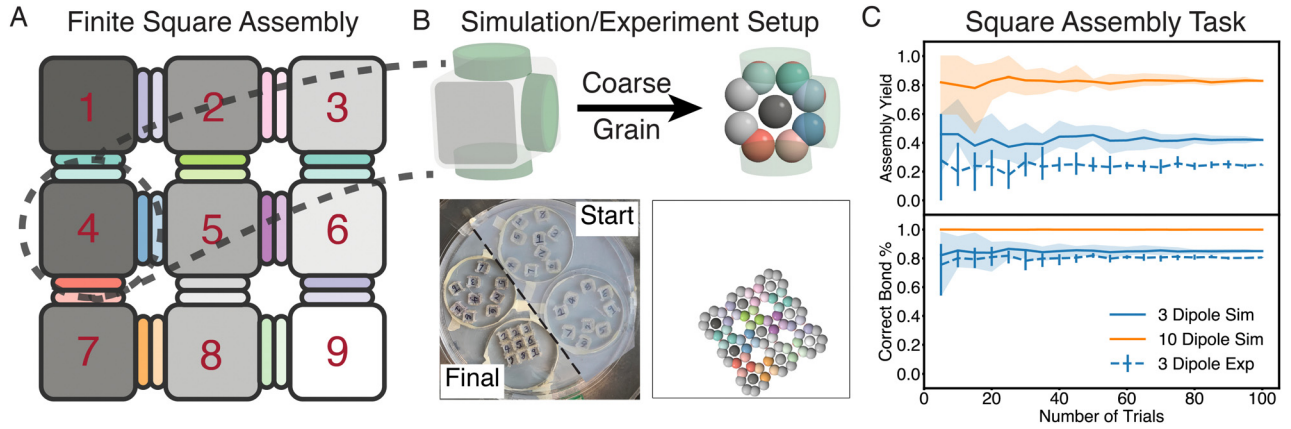

Fig. 5 Finite square assembly: (A) Model of the 3 × 3 finite square assembly design. (B) How the fourth building block is represented in an experimental setting and how it is being coarse grained into simulation. (C) The yield of the square assembly using the designed 3-dipole panels and the 12 chosen 10-dipole panels.

0.2 comfined by an acrylic cylindrical boundary. To carry out the experiment, we start the shaker at high shaking acceleration to thermalize the panels, and slowly decrease the shaking acceleration to a target amplitude where we count the number of correctly and incorrectly assembled dimers (Fig. 4E and F). For each shaking amplitude, we carry out five replicas of the experiment. In Fig. 4F, we see the yield of dimer assembly from the shaker experiment. The highest yield is around 80%, which agrees with simulation (Fig. 4D).

We note a decrease in yield at lower temperature and shaking acceleration for simulation and experiments respectively. This arises from the non-equilibrium nature of the dimer self-assembly process at low temperature, where the monomers do not have the chance to freely explore space to find the optimal binding pair, but would bind with anything nearby.[39] Our dipole-pattern design strategy assumes equilibrium self-assembly process, so in order to achieve better yield at low temperatures, other strategies can be deployed.

Finite square self-assembly

To demonstrate the power of our designed interactions, we show how the magnetic panels can enable finite heterogeneous self-assembly. We aim to self-assemble a finite 3 × 3 square (Fig. 5A), using 12 different lock key pairs to encode each of the required binding sites. We instantiate this both using the 12 patterns from the 3-dipole system discussed above, and compare this to a selection of 12 10-dipole patterns (see ESI† for panel patterns) generated following the $d/a = \sqrt{2}/2$ design rule. We selected these 12 10-dipole patterns by identifying the top 12 highest information content patterns from 150 different ones. For the simulations, we encode the required binding strengths as binding sites on spheres with attractive patches, with each square building block modeled with a rigid assembly of spheres (Fig. 5B). We first find the optimal temperature for the highest correct binding lock-key pairs by sweeping through a range of different temperatures, and ran 100 independent replica runs at the optimal temperature to measure the yield. Fig. 5C shows the measured percentage of complete square assembly (blue solid line) and correct bonds (yellow solid line) in our simulation. The correct bond yield is approximately 83%, consistent with our dimer self-assembly. The yield of perfectly assembled squares is closer to 40%, with the majority of the errors arising from assemblies with 7 correctly assembled squares, one square having an incorrect bond and one free square. The 10-dipole panels are significantly more accurate, with the success rate of complete square assembly increasing from 40% to 80%, and nearly 100% rate of correct bonds.

We also carried out experiments for assembling this configuration using panels with three dipole patterns and the shaker. Similar to simulation, we first performed the shaker experiment at different shaking acceleration to identify the optimal amplitude for square assembly (see experimental details in ESI†), and we repeated the experiment 100 times at the optimal shaking amplitude. These experiments yielded a correct bond rate of 80%, whereas 25 out of 100 runs led to perfectly assembled configurations. The correct bond rate is similar to that seen in the dimer experiment and the simulations, while the experimental yield is slightly lower.

4 Discussion

We demonstrate in this paper a simple design rule for maximizing the mutual information between lock and key pairs. By fixing $d/a = \sqrt{2}/2$, we maximize the dipole density while minimizing both the cross talk between off-target binding pairs and the distribution width for on-target binding energy over the entire set of dipole patterns. Strikingly, our calculations demonstrate that for two dimensional panels, we increase the programmability by printing more magnetic dipoles, each of which has weaker binding strength. Magnetic handshake materials allow us to take full advantage of this design rule, as we can precisely control the strength and the location of the single dipole domains being printed. Moreover, by printing the dipole patterns on two dimensional surfaces – in contrast to one

dimensional chains of *e.g.* DNA – we can increase the amount of information that can be encoded in a given building block (Fig. 3C). Finally, implementation of our theoretical designs for self-assembly in mm-sized magnetic panels, highlights their applicability to real experimental systems.

It is interesting to speculate about the number of potential lock-key pairs that can be created using state of the art nanofabrication technology. Fig. 3C shows that the number of effective non-crosstalk patterns scale super linearly with the number of dipole domains. In scaling magnetic handshake materials down to micron-scale panels, it is important to consider the maximum achievable density of non-crosstalking lock-key pairs (M_c) given state-of-the-art magnetic recording technology. The current areal bit density of perpendicular magnetic recording media, where one bit represents a magnetic moment oriented into or out of the plane of the disk, is on the order of 1Tb/in^2.[40] At this density, one bit comprises an area of 645 nm^2, with typical recording layer thicknesses of 10–30 nm.[41] Setting the interaction distance d between two panels as the bit thickness, our d/a design rule dictates a nearest neighbor distance a = 14–32 nm. With these constraints, we determine current recording technology could easily achieve a density on the order of hundreds of non-crosstalking lock-key interactions, M_c, per 1 um^2 panels. Thus, magnetic handshake materials offer a new powerful pathway towards the rapid design and creation of programmable interactions for self-assembly of increasingly complex structures.

Author contributions

C. X. D., H. A. Z., T. P., P. L. M., I. C. and M. P. B. designed research; C. X. D., H. A. Z. and J. N. performed research; C. X. D. and M. P. B. contributed new reagents/analytic tools; C. X. D. and H. A. Z. analyzed data; and C. X. D., H. A. Z., T. P. and M. P. B. wrote the paper.

Conflicts of interest

There are no conflicts of interest to declare.

Acknowledgements

This work was supported by NSF Grants DMR-1921567 and DMR-1921619, Office of Naval Research through ONR N00014-17-1-3029, the Sloan Foundation Matter to Life program award 137070-20834, the Simons Foundation and partially supported by the Cornell Center for Materials Research Grant DMR-1719875. The computations in this paper were run on the FASRC Cannon cluster supported by the FAS Division of Science Research Computing Group at Harvard University.

Notes and references

1 M. E. Johnson and G. Hummer, *Proc. Natl. Acad. Sci. U. S. A.*, 2011, **108**, 603–608.
2 C. M. Dobson, *Nature*, 2003, **426**, 884–890.
3 K. A. Dill and J. L. MacCallum, *Science*, 2012, **338**, 1042–1046.
4 T. Kirchhausen, *Annu. Rev. Biochem.*, 2000, **69**, 699–727.
5 Q. Luo, C. Hou, Y. Bai, R. Wang and J. Liu, *Chem. Rev.*, 2016, **116**, 13571–13632.
6 E. R. Kay and D. A. Leigh, *Angew. Chem., Int. Ed.*, 2015, **54**, 10080–10088.
7 S. Erbas-Cakmak, D. A. Leigh, C. T. McTernan and A. L. Nussbaumer, *Chem. Rev.*, 2015, **115**, 10081–10206.
8 S. M. Douglas, H. Dietz, T. Liedl, B. Högberg, F. Graf and W. M. Shih, *Nature*, 2009, **459**, 414–418.
9 K. F. Wagenbauer, C. Sigl and H. Dietz, *Nature*, 2017, **552**, 78–83.
10 M. A. Boles, M. Engel and D. V. Talapin, *Chem. Rev.*, 2016, **116**, 11220–11289.
11 M. R. Jones, N. C. Seeman and C. A. Mirkin, *Science*, 2015, **347**, 1260901.
12 Y. Wang, Y. Wang, X. Zheng, É. Ducrot, J. S. Yodh, M. Weck and D. J. Pine, *Nat. Commun.*, 2015, **6**, 1–8.
13 W. B. Rogers, W. M. Shih and V. N. Manoharan, *Nat. Rev. Mater.*, 2016, **1**, 1–14.
14 R. Niu, C. X. Du, E. Esposito, J. Ng, M. P. Brenner, P. L. McEuen and I. Cohen, *Proc. Natl. Acad. Sci. U. S. A.*, 2019, **116**, 24402–24407.
15 A. Moser, K. Takano, D. T. Margulies, M. Albrecht, Y. Sonobe, Y. Ikeda, S. Sun and E. E. Fullerton, *J. Phys. D: Appl. Phys.*, 2002, **35**, R157.
16 K. J. Dorsey, T. G. Pearson, E. Esposito, S. Russell, B. Bircan, Y. Han, M. Z. Miskin, D. A. Muller, I. Cohen and P. L. McEuen, *Adv. Mater.*, 2019, **31**, 1901944.
17 J. Cui, T.-Y. Huang, Z. Luo, P. Testa, H. Gu, X.-Z. Chen, B. J. Nelson and L. J. Heyderman, *Nature*, 2019, **575**, 164–168.
18 W.-H. Hsu, PhD thesis, University of Minnesota, 2021.
19 D. Weller and A. Moser, *IEEE Trans. Magn.*, 1999, **35**, 4423–4439.
20 H. Richter, *IEEE Trans. Magn.*, 1999, **35**, 2790–2795.
21 H. Richter, A. Lyberatos, U. Nowak, R. F. L. Evans and R. W. Chantrell, *J. Appl. Phys.*, 2012, **111**, 033909.
22 W. Wen, F. Kun, K. F. Pál, D. Zheng and K.-N. Tu, *Phys. Rev. E: Stat. Phys., Plasmas, Fluids, Relat. Interdiscip. Top.*, 1999, **59**, R4758.
23 J. Stambaugh, D. P. Lathrop, E. Ott and W. Losert, *Phys. Rev. E: Stat., Nonlinear, Soft Matter Phys.*, 2003, **68**, 026207.
24 J. Stambaugh, Z. Smith, E. Ott and W. Losert, *Phys. Rev. E: Stat., Nonlinear, Soft Matter Phys.*, 2004, **70**, 031304.
25 A. Snezhko, I. Aranson and W.-K. Kwok, *Phys. Rev. Lett.*, 2005, **94**, 108002.
26 D. L. Blair and A. Kudrolli, *Phys. Rev. E: Stat., Nonlinear, Soft Matter Phys.*, 2003, **67**, 021302.
27 S. Kantorovich, J. J. Cerda and C. Holm, *Phys. Chem. Chem. Phys.*, 2008, **10**, 1883–1895.
28 A. Kögel, P. A. Sánchez, R. Maretzki, T. Dumont, E. S. Pyanzina, S. S. Kantorovich and R. Richter, *Soft Matter*, 2018, **14**, 1001–1015.
29 P. A. Sánchez, J. Miller, S. S. Kantorovich and R. Richter, *J. Magn. Magn. Mater.*, 2020, **499**, 166182.
30 S. Kantorovich, E. Pyanzina and F. Sciortino, *Soft Matter*, 2013, **9**, 6594–6603.
31 M. H. Huntley, A. Murugan and M. P. Brenner, *Proc. Natl. Acad. Sci. U. S. A.*, 2016, **113**, 5841–5846.

32 V. Danilov, T. Prokopyeva and S. Kantorovich, *Phys. Rev. E: Stat., Nonlinear, Soft Matter Phys.*, 2012, **86**, 061408.
33 J. A. Anderson, J. Glaser and S. C. Glotzer, *Comput. Mater. Sci.*, 2020, **173**, 109363.
34 T. D. Nguyen, C. L. Phillips, J. A. Anderson and S. C. Glotzer, *Comput. Phys. Commun.*, 2011, **182**, 2307–2313.
35 J. Glaser, X. Zha, J. A. Anderson, S. C. Glotzer and A. Travesset, *Comput. Mater. Sci.*, 2020, **173**, 109430.
36 V. Ramasubramani, B. D. Dice, E. S. Harper, M. P. Spellings, J. A. Anderson and S. C. Glotzer, *Comput. Phys. Commun.*, 2020, **254**, 107275.
37 C. S. Adorf, P. M. Dodd, V. Ramasubramani and S. C. Glotzer, *Comput. Mater. Sci.*, 2018, **146**, 220–229.
38 V. Ramasubramani, C. S. Adorf, P. M. Dodd, B. D. Dice and S. C. Glotzer, Proceedings of the 17th Python in Science Conference, 2018, pp. 152–159.
39 M. Williams, *Phys. Rev. E: Stat., Nonlinear, Soft Matter Phys.*, 2019, **99**, 042133.
40 B. Marchon, T. Pitchford, Y.-T. Hsia and S. Gangopadhyay, *Adv. Tribol.*, 2013, **2013**, 521086.
41 W.-H. Hsu and R. Victora, *Appl. Phys. Lett.*, 2021, **118**, 072406.

